https://doi.org/10.15302/frontphys.2025.012201

LETTER

Manipulating macroscopic curved objects by light

Gui-hua Chen[1,2], Mu-ying Wu[1], Yong-qing Li[1,3,†]

[1]School of Electronic Engineering & Intelligentization, Dongguan University of Technology, Dongguan 523808, China
[2]Institute of Science & Technology Innovation, Dongguan University of Technology, Dongguan 523808, China
[3]Department of Physics, East Carolina University, Greenville, North Carolina 27858-4353, USA
Corresponding author. E-mail: †liy@ecu.edu
Received August 21, 2024; accepted September 1, 2024

Supplementary Information

Part 1: Materials and methods, and supplementary experiments

Laser pulling and pushing of a cylindrical metal vane. The absorbing cylindrical vane was made of a thin aluminum sheet (8 mm×8 mm in size and 15 μm in thickness), which was painted with Black 2.0 paint on both sides and bended into the cylindrical shape with a cylindrical rod of a specific radius. The cylindrical aluminum vane was suspended with an ultra-fine copper wire (70 mm in length and 10 μm in diameter) to form a pendulum inside a vacuum chamber (15 cm in height and 12 cm in diameter), see Fig. 1(a). The pressure of the vacuum chamber was controlled with a Turbo pump station and a set of valves, which were closed off during the experiment such that there was no air flow inside the chamber while the pressure in the chamber was maintained at constant. A continuous-wave collimated laser beam at 450 nm (with a beam size of ~2 mm×4 mm and the maximum power of 1.2 W) was incident on the concave or convex side of the absorbing cylindrical vane. The temperature of the absorbing surface was measured to be ~50 ºC higher than that of the vacuum chamber with an infrared thermometer. Upon the illumination of the laser beam, the absorbing aluminum vane was deflected from its equilibrium position, which was recorded with a video camera. The deflection angle was determined by the ratio of the displacement and the string length, and the mass (and gravitational force) of the vane was determined by the known density and volume of the aluminum vane. See Online Supplementary Video S1. Figure S1 shows the deflection angle of the pendulum as the function of the illumination laser power.

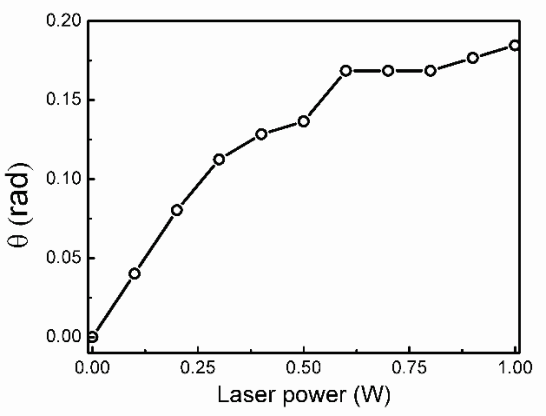

Fig. S1 Angular displacement of the pendulum as the function of laser power. The light-absorbing cylindrical aluminum vane (8×8 mm in size and 15 μm in thickness) is suspended with an ultrafine copper string in a pendulum and is pulled towards the laser beam. The central angle of the vane is 180º at the pressure of 0.1 Torr.

Laser lifting of a cylindrical metal vane. An ultrathin gold foil leaf (7 mm×7 mm in size and ~0.2 μm in thickness) was painted with Black 2.0 paint and gently bended into the cylindrical surface. The cylindrical gold leaf was placed

on the top of a flat surface with four contact points and with the concave side facing up [see Fig. S2(b)]. The pressure of the vacuum chamber (a 10 mm×10 mm×50 mm quartz cuvette cell or a large jar chamber) was controlled with a Turbo pump station. When the illuminating laser beam of 1 W at 650 nm was turned on, the absorbing gold leaf was rapidly lifted up, which was recorded with a slow-motion video camera (240 fps), see Online Supplementary Video S2. A green short-pass filter was used in the front of the camera to block the scattered laser light.

In Figs. S2 and S3, we show that the attractive radiometric force is large enough to overcome the gravitational force F_G and lift ultrathin curved gold vanes off the ground by the laser illumination. F_G of the curved gold leaf is estimated to be 1.85 μN from the known density and volume of the vane. The vane can be quickly pulled off from the supporting surface and lifted up until the top of the vacuum chamber in ~40 ms by the attractive F_{RM}, see Supplementary Video S2.

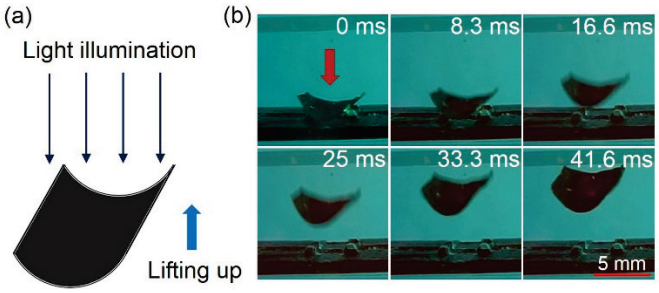

Fig. S2 An example of lifting a curved vane. **(a)** An ultrathin curved vane is lifted when the concave side is illuminated. **(b)** Time-lapsed images of a cylindrical gold leaf (with 7 mm×7 mm in size and 0.2 μm in thickness) when the laser beam is turned on. The laser power is 1 W at 650 nm and the pressure is 0.3 Torr.

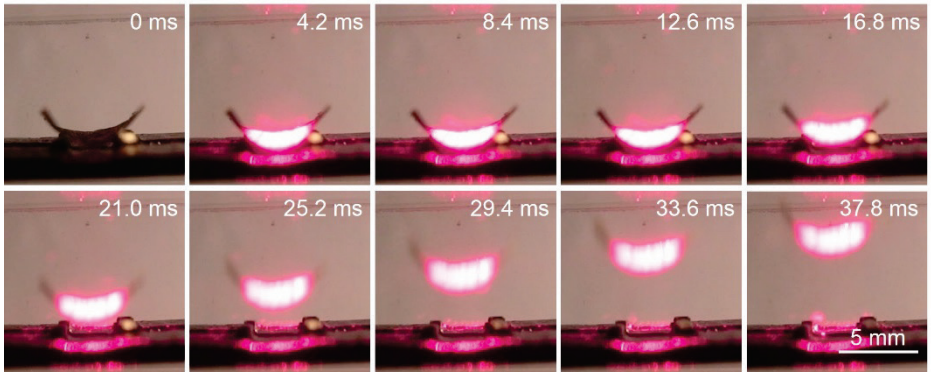

Fig. S3 Another example of lifting a cylindrical gold leaf. Time-lapsed images of a cylindrical gold leaf (7 mm×7 mm in size, 0.2 μm in thickness) when illuminated by a laser power at 650 nm with an optical power of 1 W under the pressure of 0.3 Torr.

The radiometric force acting on the curved vane observed in the lifting experiment appears to be some similar with the Knudsen force, which is the radiometric force generated between the two plates kept at different temperatures, which are typically separated by a distance comparable to a mean free path of the molecules of the ambient medium [20,26,27]. The Knudsen force was first observed in a Nichols radiometer, which consists of two plates, one being a suspended vane, and the second being the wall of the container, with a very small air gap between the vane and container wall [20]. Once the vane is uniformly heated, the vane moves to or from the wall, depending on whether the vane is hotter or colder than the chamber wall [20]. Passian *et al.* [26] also demonstrated the Knudsen force on a light-heated microcantilever adjacent to a cold substrate surface during thermal transpiration. The small gap between the heated microplate and the substrate confines the ambient gas molecules in this region. In free-molecular regime, the collisions of the confined gas molecules with the heated microplate reduce thermal gradient of the gas in the gap, comparing to the thermal gradient on other side of the microplate. This leads to a Knudsen force on the heated microplate pointing towards the side with a lower thermal gradient [27]. This picture is similar to Maxwell's

interpretation of Crooke's observation of the attractive force on cup-shaped vanes [19, 36]. Maxwell considered that the thermal gradient on the concave side is smaller than that on the convex side of a cup-shaped vane, probably due to the partially gas confinement on the concave side. Hence the normal pressure will be greater on the convex surface than on the concave surface under free-molecular regime [19].

However, the experiments in our work show that the generation of radiometric force on a heated curved vane does not require the presence of a substrate or a container wall at a different temperature and in a short separation distance to confine the gas molecules, which are two necessary conditions required to generate the Knudsen force. In our pendulum experiment, the distance between the suspended curved vane and the wall of the container is very large (much larger than the mean free path of the gas molecules inside the container), and the curved vane could be pulled in free space with a rarefied gas at low pressure. It should be noted that in the experiment of lifting a curved vane the gas confinement on the convex side by the supporting substant is also not required. In addition, during the experiment we found that when the illumination laser is turned on the lifted curved vane can stay at the top of the vacuum chamber for a long time, and when the illumination laser is turned off the lifted curved vane falls off. Therefore, the confinement effect of the substrate on the gas is obviously negligible in our experiment. In other words, the radiometric force caused by the bending of the vane is sufficient to overcome its gravity and lift the curved vane.

Laser pulling of Crookes radiometer with four-curved vanes. The black cylindrical curved vane was made with matte black aluminum sheet (16 mm×16 mm in size and 50 μm in thickness, Cinefoil, Rosco Corp.). Four curved vanes were mounted on a small glass tube [see Fig. 4(a)], which was placed on the top of a stainless-steel needle to allow for rotation in a vacuum chamber with the minimized resistance. A collimated laser beam at 650 nm (with a beam size of ~5 mm×5 mm) was incident on the concave or convex side of one curved vane and drive the rotation of the Crookes radiometer. A video camera was used to record the rotation with a 550-nm short-pass filter inserted in the front of the camera to block the laser scattering light, see Online Supplementary Video S3. A photodiode was used to detect the attenuated laser beam that passed through the vanes and the rotation speed was determined from the periodic photodiode signal.

Figure S4 shows the dependence of the rotation speed of a Crookes radiometer with four curved vanes on central angle and gas pressure. The maximum rotation speed of a Crookes radiometer with four-curved vanes (10 mm×10 mm in size and 50 μm in thickness) was ~650 rpm with the laser power of 1 W and the pressure of 0.03 Torr.

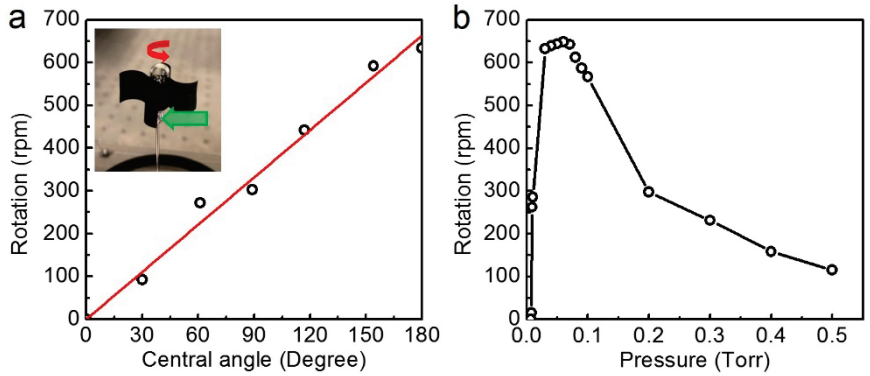

Fig. S4 Dependence of rotation speed of a Crookes radiometer with four curved vanes on central angle and gas pressure. **(a)** Dependence of rotation speed on central angle Θ_0 of the curved vane (10 mm×10 mm in size and 50 μm in thickness, shown in the insert). The laser power is 1 W and the pressure is 0.03 Torr. The rotation speed is proportional to the central angle of the vanes (fit in line). **(b)** Dependence of rotation speed on the pressure with the central angle $\Theta_0=\pi$.

Part 2: The effect of multiple reflections on pressure force F_n acting on a curved vane

The pressure force F_n acting on a curved vane due to the collision of gas molecules is generated by the unbalanced momentum flux between the molecules leaving the concave and convex sides of the vane and acts in the direction towards the concave side [see Fig. S5]. As shown in Fig. S5(b), in free-molecular regime (Kn>10 at low gas pressure), all molecules hitting on a surface element ΔS from the convex side (such as molecule 1) only experience single

reflection on the surface, leaving at a higher temperature T with the difference of $T–T_0=\alpha(T_s–T_0)$, where α is the accommodation coefficient of the surface which is assumed to be uniform on the whole vane, T_0 the temperature of a rarefied gas and T_s the temperature of the heated vane ($T_0<T_s$). However, some molecules hitting on ΔS from the concave side (such as molecule 2) experience two or multiple reflections on the surface, thus leaving with a temperature difference of $T–T_1=\alpha(T_s–T_0)–\alpha^2(T_s–T_0)$, where $T_1=T_0+\alpha(T_s–T_0)$ is the molecule's temperature before hitting on ΔS due to the first reflection. As a result, the energy difference between a pair of molecules (e.g., molecules 1 and 2) leaving ΔS is $\Delta E=\alpha^2k(T_s–T_0)$, leading to a net momentum change pointing from the convex to the concave sides, where k is Boltzmann constant. Note that the molecule flux hitting on ΔS from both sides should be identical because F_n should be zero if there is no temperature difference between the vane and surrounding molecules. The effect of the first hitting of molecule 2 on the concave side should be cancelled by the hitting of other molecule on the convex side.

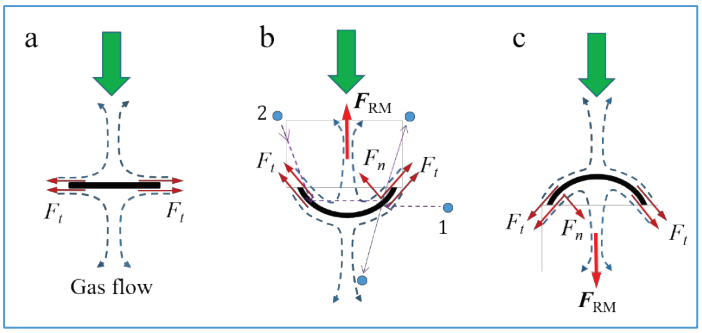

Fig. S5 Schematic showing the tangential shear force and pressure force on a hot curved vane. **(a)** Schematic showing tangential shear forces on the surface of a hot flat vane due to gas flow. The net F_{RM} on the vane is zero due to the geometry balance. **(b)** Pressure force and shear force on a surface element of a concave vane and the total F_{RM} pointing to the upward direction. Single collision of the incident molecules occurs on the convex side, and twice or multiple collisions of the incident molecules occur on the concave side. **(c)** Pressure force and shear force on a surface element of a convex vane and the total F_{RM} pointing to the downward direction.

Part 3: Numerical simulation

The flow characteristics of the gas fluid near the curved vane. The fluid near the curved vane in our experiment has the characteristics of slip flow. To study the gas dynamic behavior, four different regimes are generally distinguished by the dimensionless Knudsen number Kn ($=\lambda/W$), the ratio of the mean free path λ of the molecules and the dimension W of the flow field or the body in the flow field [37,38]. These four regimes are (i) the continuum flow regime, $Kn<0.001$; (ii) the slip flow regime, $0.001<Kn\leq0.1$; (iii) the transitional flow regime, $0.1<Kn<10$; and (iv) the free molecular flow regime, $Kn\geq10$. In our experiment, a single cylindrical vane (8 mm×8 mm in size and 15 μm in thickness) is suspended with an ultrafine copper wire as a pendulum in a vacuum chamber (with a radius of 60 mm and a height of 150 mm) and illuminated by a light beam. The photon energy of the illumination light is absorbed by Black 2.0 paint [39] on one side and transferred by thermal conduction to the metal vane, resulting in both sides of the vane heated to an identical temperature since the used aluminum or gold vanes are extremely thin and excellent thermal conductors. We directly observe a light-induced attraction or repulsion radiometric force (F_{RM}) acting on a thin absorbing curved metal vane. Therefore, F_{RM} acting on a curved metal vane should be the second type of radiometric force caused by unbalanced heat exchange between two surfaces of the vane and the gas molecules, due to the curved surface geometry. The experimental results show that the pressure range in which a significant radiometric force is produced is from 0.05 to 1.0 Torr. With the size of the vane (~10 mm) taken as the characteristic length, the Kn value corresponds to 0.1–0.005, which is in the slip flow regime. In this regime the flow is governed by the Navier–Stokes equations, and the rarefaction effects are modeled through the partial slip at the wall using Maxwell's velocity slip and Smoluchowski's temperature jump boundary conditions [40]. Therefore, the modified Navier-Stokes equations can be used to describe the characteristics of the gas flow near the curved metal vane.

The model. According to the size of the vane and the pressure range in which a significant radiometric force is produced, the air near the curved vane in our experiment has the characteristics of slip flow, and can be described by the Navier–Stokes equations as follows [40]:

$$\frac{\partial \rho}{\partial t} + \nabla \cdot (\rho \boldsymbol{u}) = 0, \tag{1}$$

$$\frac{\partial \rho \boldsymbol{u}}{\partial t} + \nabla \cdot (\rho \boldsymbol{u}\boldsymbol{u}) = -\nabla p + \nabla \cdot \mathbf{K} + \boldsymbol{F}, \tag{2}$$

$$\frac{\partial}{\partial t}\left[\rho\left(e + \frac{1}{2}u^2\right)\right] + \nabla \cdot \left[\rho \boldsymbol{u}\left(e + \frac{1}{2}u^2\right)\right] = -\nabla \cdot \boldsymbol{q} + \nabla \cdot (-p\boldsymbol{u} + \mathbf{K} \cdot \boldsymbol{u}) + \boldsymbol{u} \cdot \boldsymbol{F} + Q. \tag{3}$$

Equations (1)–(3) correspond respectively to the conservation equations of mass, momentum and energy for a fluid element, in which ρ is the density, p is the pressure, e is the internal energy per unit mass, $\boldsymbol{u}$ is velocity vector, u^2 is the square of the velocity magnitude, $\boldsymbol{q}$ $(= -k\nabla T)$ is the heat flux vector, $\mathbf{K}$ is the viscous stress tensor, $\boldsymbol{F}$ is a volumetric force per unit mass (such as gravity or electromagnetic force, etc.), and Q is the heat produced by illumination of laser beam on the vane.

It is worthy to note that, by considering the relationship between internal energy and temperature T, Eq. (3) can be written as the equation of temperature with the help of Eq. (1):

$$\rho C_p \frac{\partial T}{\partial t} + \rho C_p \boldsymbol{u} \cdot \nabla T = -\nabla \cdot \boldsymbol{q} + \left(\frac{\partial p}{\partial t} + \boldsymbol{u} \cdot \nabla p\right) + \mathbf{K} : \nabla \boldsymbol{u} + Q. \tag{4}$$

When the system reaches a steady state, Eqs. (1), (2) and (4) are simplified as follows:

$$\nabla \cdot (\rho \boldsymbol{u}) = 0, \tag{5}$$

$$\nabla \cdot (\rho \boldsymbol{u}\boldsymbol{u}) = -\nabla p + \nabla \cdot \mathbf{K} + \boldsymbol{F}, \tag{6}$$

$$\rho C_p \boldsymbol{u} \cdot \nabla T = -\nabla \cdot \boldsymbol{q} + \boldsymbol{u} \cdot \nabla p + \mathbf{K} : \nabla \boldsymbol{u} + Q. \tag{7}$$

Because the air in the system is in the slip flow regime, there are obvious velocity slip and temperature jump of the gas molecules on the surface of the vane. In order to describe the behavior of the air molecules more accurately, we need to modify the slip velocity and temperature of the air near the vane surface and use them as boundary conditions to solve the above equations. It should be pointed out that this method is not as strict as the Boltzmann equation or its simplified form (such as BGK equation), but it is relatively easy to deal with, and the solution results usually meet the accuracy requirements of engineering calculation.

The boundary conditions for the slip velocity and temperature of the air near the surface of the vane are given by the following two equations [40]:

$$\boldsymbol{u}_{\text{slip}} = \sigma_s \frac{\lambda}{\mu}\{\mathbf{K} \cdot \boldsymbol{n} - [(\boldsymbol{n}^T \mathbf{K} \boldsymbol{n})\boldsymbol{n}]\} + \sigma_T \frac{\mu}{\rho T_g}[\nabla T_v - (\boldsymbol{n} \cdot \nabla T_v)\boldsymbol{n}], \tag{8}$$

$$T_v = T_g - \zeta_T \lambda \boldsymbol{n} \cdot \nabla T_g, \tag{9}$$

where λ is the mean free path of the gas, $\boldsymbol{n}$ is the normal unit vector of the boundary, T_v is the surface temperature of the vane (since the thermal conductivity of aluminum is very good and the thickness of the vane is very small, we assume that the temperature of the vane is uniform everywhere), T_g is the temperature of the gas, μ is the viscosity of the gas, ρ is the density of the gas, σ_s (viscous slip coefficient), σ_T (thermal slip coefficient) and ζ_T (temperature jump coefficient) is collectively referred to as slip coefficient, which can be defined by material properties and tangential momentum accommodation coefficient α. In Maxwell's model, the slip coefficient (σ_s, σ_T and ζ_T) and the tangential momentum accommodation coefficient α satisfy the following relation:

$$\sigma_s = \frac{2-\alpha}{\alpha}, \tag{10}$$

$$\sigma_T = \frac{3}{4}, \tag{11}$$

$$\zeta_T = 2\frac{2-\alpha}{\alpha}\frac{\gamma}{\gamma+1}\frac{\kappa}{\mu C_p}, \tag{12}$$

where κ is the thermal conductivity of air, γ is the specific heat capacity ratio of air, C_p is the molar heat capacity at constant pressure. The mean free path of air can be calculated from the gas characteristics using the following formula:

$$\lambda = \frac{1}{C_0}\frac{\mu}{\rho\bar{v}}, \tag{13}$$

$$\bar{v} = \left(\frac{8RT}{\pi M_n}\right)^{1/2} = \left(\frac{8p}{\pi\rho}\right)^{1/2}, \tag{14}$$

where M_n is the molar mass of air, C_0 is a constant, ranging $0.491 \leq C_0 \leq 0.499$ for rarefied gases.

Results and discussion. By using COMSOL multiphysics™ simulation software, we simulate the dynamic behavior of the air surrounding the vane with different bending degrees by solving Eqs. (5)–(7) with the boundary condition [Eqs. (8) and (9)], and obtain the velocity and temperature distributions of the gas. In our simulation, a light-absorbing aluminum sheet with its dimension of 10 mm×10 mm×0.1 mm is bent into cylindrical surfaces with different central angles and placed in the center of a glass chamber with its dimension of 100 mm×100 mm×100 mm and the chamber's wall thickness of 3 mm. It is assumed that the heat transferred to the outer surface of the glass chamber is rapidly dissipated to the outer space. In order to simulate the interaction between the vane heated by the incident laser and the surrounding air, we set the vane as the internal heat source in the program with its power taking the incident laser power (0.7 W). The initial pressure of air in the chamber is set as 0.1 Torr, and the initial temperature is set as 20 ℃. As an important parameter to describe the interaction between gas and solid, the value of thermal accommodation coefficient is dependent on several parameters including nature of the gas, pressure of the gas, material of the surface, surface cleanliness and roughness, and surface temperature [41]. The values of thermal accommodation coefficient between air and other solid surfaces and between various gases and aluminum surface range from 0.7 to 1.0 [42,43]. Without losing generality, in our program, the thermal accommodation coefficient between air and aluminum surface is taken as 0.9. We focus on the effects caused by the bending of the vane (for example, the influence of airflow near the vane on the radiometric force). Here we simulate the interaction between the surrounding air and the cylindrical vane with its center angle of 0°, 90° and 180° respectively (assuming that the central axis of the curved vane is parallel to the *Z* axis), and obtain the distribution of air velocity and air temperature near the vane. Since the vane does not bend in the direction parallel to the *Z* axis, the influence of bending effect on the radiometric force is more obvious in the plane perpendicular to the *Z* axis. Therefore, we only show the distribution of air velocity and air temperature near the vane on the *XY* plane which is perpendicular to the *Z* axis and bisects the vane, and the results are shown in Fig. 3.

Figures 3(a), (c) and (e) show the distribution of air velocity near cylindrical vanes with center angle of 0°, 90° and 180° respectively, in which the lines show the flow direction of the gas, and the color represents the magnitude of flow velocity. It can be seen from these panels that the gas flows into the vane from the upper and lower sides of the vanes, and flows out from the left and right sides of the vanes, which is consistent with the result reported by Taguchi *et al*. [44]. The region with fast velocity appears at the upper and lower ends of the vanes, while the region with slow velocity appears in the middle area of the vanes. Comparing the velocity distribution of three vanes, we can find that the curved vanes squeeze the gas flow on the concave side and makes it forming vortex in the local space near the vane. The more curvature the vane is, the more localization the vortex distribution is. In the curved vane with the center angle of 180°, part of the gas seems to be confined in the local space of the concave side and these molecules are difficult to escape.

The temperature distribution of the air near the vanes with center angle of 0°, 90° and 180° can also be simulated and shown in Fig. 4(b), (d) and (f), respectively. It is easy to understand the temperature distribution from the velocity distribution of the airflow. For the flat vane, because the velocity distribution on both sides is identical due to the geometrical symmetry, the temperature distribution on both sides also has a similar bilateral symmetry. For the curved vanes, a part of the gas is squeezed on the concave side and cannot exchange heat with the gas far away from the vane by convection. Thus, the gas temperature on the concave side is higher than that on the convex side. The more curvature the vane is bent, the stronger the confinement effect is.

Following the procedure proposed by Scandurra *et al*. [35], the Chapman–Enskog method is used to obtain analytical formula for net pressure force (where we ignore the contribution of molecules in thermal equilibrium to the pressure on the surface of the vane with the assumption that the product nT is constant throughout the gas [35,40,45]) and for shear force on the unit area of the vane surface due to the gas temperature differences near the interface under the condition of Kn < 1, as follows:

$$\Delta p_{\mathrm{norm}} = (2-\alpha)\frac{15k}{32\sqrt{2}\pi\sigma^2}\frac{dT}{dx_n}, \tag{15}$$

$$\Delta p_{\mathrm{shear}} = -\alpha\frac{15k}{64\sqrt{2}\pi\sigma^2}\frac{dT}{dx_t}, \tag{16}$$

where α is the tangential momentum accommodation coefficient, k is the Boltzmann constant, $\pi\sigma^2$ is the collision cross-sectional area of gas molecules, $\mathrm{d}T/\mathrm{d}x_n$ and $\mathrm{d}T/\mathrm{d}x_t$ denotes the gas temperature gradients perpendicular to the vane surface and parallel to the vane surface, respectively. Due to the equivalence of Boltzmann equations and continuity equations in describing the macroscopic properties of the system in the slip flow region, we can use Eqs. (15) and (16) to calculate the net pressure force and shear force on the concave and convex surfaces of the vane, and obtain the total radiometric force. We focus on the relationship between the radiometric force and the bending degree, and the results are shown in Fig. S6. Compared with the experimental result [see Fig. 1(e)], it is not difficult to find that the theoretical simulation result can reflect well the influence of the bending on the radiometric force.

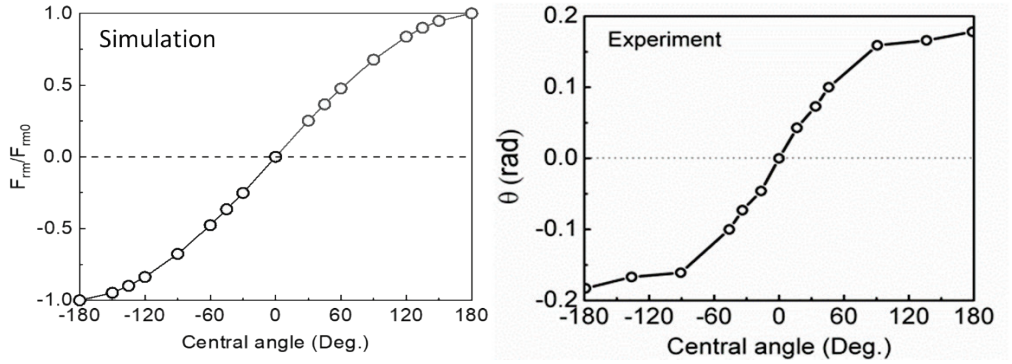

Fig. S6 The simulated dependence of the radiometric force acting on the vanes on different degrees of bending (center angles) under the laser irradiation with a fixed incident power (0.7 W). Here, F_{rm0} is the radiometric force on the vane with its center angle of 180°.

As mentioned in the text, we interpret the observed radiometric force on a vane by the combination of pressure force and shear force. For the flat vane, the shear forces acting on the front and rear surfaces of the vane are balanced, so people seldom discuss them. After bending the vane, the shear force can be displayed. Figure S7 shows the ratios of net pressure force and shear force to the total radiometric force, as well as their variation with bending degree of the vane. It can be seen from the figure that the shear force has the same order of magnitude as the net pressure force, and the former is about half of the latter.

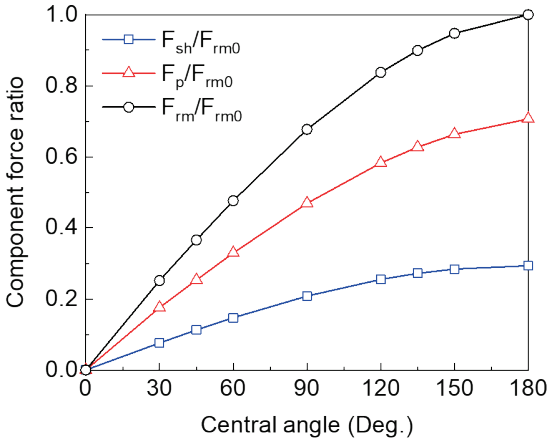

Fig. S7 The ratios of net pressure force F_p (or F_n) and shear force F_{sh} (or F_t) to the total radiometric force F_{RM}, as well as their variation with bending degree of the vane. Laser irradiation is kept at a fixed incident power (0.7 W) and the air pressure is kept at 0.1 Torr. Here, F_{rm0} is the radiometric force on the vane with its center angle of 180°.

Part 4: Supplementary movies

Supplementary Video S1: Macroscopic observation of the deflection and restoration of a suspended curved vane when the laser beam is turned on and off.

Supplementary Video S2: Macroscopic observation of the rotation of a Crookes radiometer with four-curved vanes driven by an attractive radiometric force when a laser beam at 450 nm with an optical power of 0.8 W is incident on the vane under the pressure of 0.02 Torr. When the laser beam is turned on, the radiometer starts the rotation and reaches the maximum speed in about 1 min. When the laser beam is turned off, the radiometer decelerates and stops in about 1 min.

Supplementary Video S3: Macroscopic observation of the lifting of a curved gold leaf by an attractive radiometric force when a laser beam at 650 nm with an optical power of 1 W is incident on the vane under the pressure of 0.3 Torr.

References and notes

1. A. Ashkin, J. M. Dziedzic, and T. Yamane, Optical trapping and manipulation of single cells using infrared laser beams, *Nature* 330(6150), 769 (1987)

2. D. G. Grier, A revolution in optical manipulation, *Nature* 424(6950), 810 (2003)

3. J. Stajic, E. Hand, and J. Yeston, Manipulating ultracold matter, *Science* 357(6355), 984 (2017)

4. M. Wu, D. Ling, L. Ling, W. Li, and Y. Li, Stable optical trapping and sensitive characterization of nanostructures using standing-wave Raman tweezers, *Sci. Rep.* 7(1), 42930 (2017)

5. D. E. Smalley, E. Nygaard, K. Squire, J. Van Wagoner, J. Rasmussen, S. Gneiting, K. Qaderi, J. Goodsell, W. Rogers, M. Lindsey, K. Costner, A. Monk, M. Pearson, B. Haymore, and J. Peatross, A photophoretic-trap volumetric display, *Nature* 553(7689), 486 (2018)

6. J. Lu, H. Yang, L. Zhou, Y. Yang, S. Luo, Q. Li, and M. Qiu, Light-induced pulling and pushing by the synergic effect of optical force and photophoretic force, *Phys. Rev. Lett.* 118(4), 043601 (2017)

7. O. Jovanovic, Photophoresis — Light induced motion of particles suspended in gas, *J. Quant. Spectrosc. Radiat. Transf.* 110(11), 889 (2009)

8. H. Horvath, Photophoresis – a forgotten force? *Kona* 31(0), 181 (2014)

9. G. Chen, L. He, M. Wu, and Y. Li, Temporal dependence of photophoretic force optically induced on absorbing airborne particles by a power-modulated laser, *Phys. Rev. Appl.* 10(5), 054027 (2018)

10. V. G. Shvedov, A. V. Rode, Y. V. Izdebskaya, A. S. Desyatnikov, W. Krolikowski, and Y. S. Kivshar, Giant optical manipulation, *Phys. Rev. Lett.* 105(11), 118103 (2010)

11. V. Shvedov, A. R. Davoyan, C. Hnatovsky, N. Engheta, and W. Krolikowski, A long-range polarization-controlled optical tractor beam, *Nat. Photonics* 8(11), 846 (2014)

12. J. Lin, A. G. Hart, and Y. Li, Optical pulling of airborne absorbing particles and smut spores over a meter-scale distance with negative photophoretic force, *Appl. Phys. Lett.* 106(17), 171906 (2015)

13. H. Magallanes and E. Brasselet, Macroscopic direct observation of optical spin-dependent lateral forces and left-handed torques, *Nat. Photonics* 12(8), 461 (2018)

14. D. Wolfe, A. Larraza, and A. Garcia, A horizontal vane radiometer: Experiment, theory, and simulation, *Phys. Fluids* 28(3), 037103 (2016)

15. W. Crookes, XV. On attraction and repulsion resulting from radiation, *Philos. Trans. R. Soc. Lond.* 164, 501 (1874)

16. W. Crookes, On repulsion resulting from radiation. Parts III. & IV, *Philos. Trans. R. Soc. Lond*. 166, 325 (1876)

17. A. Ketsdever, N. Gimelshein, S. Gimelshein, and N. Selden, Radiometric phenomena: From the 19th to the 21st century, *Vacuum* 86(11), 1644 (2012)

18. M. Azadi, G. A. Popov, Z. Lu, A. G. Eskenazi, A. J. W. Bang, M. F. Campbell, H. Hu, and I. Bargatin, Controlled levitation of nanostructured thin films for sun-powered near-space flight, *Sci. Adv.* 7(7), eabe1127 (2021)

19. J. C. Maxwell, VII. On stresses in rarified gases arising from inequalities of temperature, *Philos. Trans. R. Soc. Lond.* 170, 231 (1879)

20. O. Reynolds, XVIII. On certain dimensional properties of matter in the gaseous state, *Philos. Trans. R. Soc. Lond.* 170, 727 (1879)

21. A. Einstein, Zur Theorie der Radiometrerkrafte, *Eur. Phys. J. A* 27(1), 1 (1924)

22. G. W. Evan, Radiometers with curved vanes, *Science* ns-2(29), 215 (1883)

23. L. H. Han, S. Wu, J. C. Condit, N. J. Kemp, T. E. Milner, M. D. Feldman, and S. Chen, Light-powered micromotor driven by geometry-assisted, asymmetric photon-heating and subsequent gas convection, *Appl. Phys. Lett.* 96(21), 213509 (2010)

24. A. D. Strongrich, W. J. O'Neill, A. G. Cofer, and A. A. Alexeenko, Experimental measurements and numerical simulations of the Knudsen force on a non-uniformly heated beam, *Vacuum* 109, 405 (2014)

25. A. Ventura, N. Gimelshein, S. Gimelshein, and A. Ketsdever, Effect of vane thickness on radiometric force, *J. Fluid Mech.* 735, 684 (2013)

26. A. Passian, R. J. Warmack, T. L. Ferrell, and T. Thundat, Thermal transpiration at the microscale: A Crookes cantilever, *Phys. Rev. Lett.* 90(12), 124503 (2003)

27. T. Zhu, W. Ye, and J. Zhang, Negative Knudsen force on heated microbeams, *Phys. Rev. E* 84(5), 056316 (2011)

28. B. M. Cornella, A. D. Ketsdever, N. E. Gimelshein, and S. F. Gimelshein, Analysis of multivane radiometer arrays in high-altitude propulsion, *J. Propuls. Power* 28(4), 831 (2012)

29. M. Young, S. Keith, and A. Pancotti, An overview of advanced concepts for near space systems, in: 45th AIAA/ASME/SAE/ASEE Joint Propulsion Conference & Exhibit, American Institute of Aeronautics and Astronautics, 2009

30. I. Levchenko, K. Bazaka, S. Mazouffre, and S. Xu, Prospects and physical mechanisms for photonic space propulsion, *Nat. Photonics* 12(11), 649 (2018)

31. R. W. Bosworth and A. D. Ketsdever, Determination of the effect of particle thermal conductivity on thermophoretic force, *AIP Conf. Proc.* 1786, 060003 (2016)

32. S. Taguchi and K. Aoki, Motion of an array of plates in a rarefied gas caused by radiometric force, *Phys. Rev. E* 91(6), 063007 (2015)

33. T. Baier, S. Hardt, V. Shahabi, and E. Roohi, Knudsen pump inspired by Crookes radiometer with a specular wall, *Phys. Rev. Fluids* 2(3), 033401 (2017)

34. The simulation was carried out on the Tianhe-2 supercomputer system of the National Supercomputing Center in Guangzhou.

35. M. Scandurra, F. Iacopetti, and P. Colona, Gas kinetic forces on thin plates in the presence of thermal gradients, *Phys. Rev. E* 75(2), 026308 (2007)

36. W. Crookes, I. Experimental contributions to the theory of the radiometer - Preliminary notice, *Proc. R. Soc. Lond*. 25, 304 (1876)

37. H.-S. Tsien, Superaerodynamics, the mechanics of rarefied gases, *J. Aeronaut. Sci.* 13, 653 (1964)

38. F. M. Devienne, Low density heat transfer, in: J. P. Hartnett, T. F. Irvine, Jr. (Eds.), Advances in heat transfer, Vol. 2, New York: Academic Press, 1965, pp 271-356

39. The specification of Black 2.0 is available on: www.culturehustleusa.com/products/black-v1-0-beta-the-world-s-mattest-flattest-blackest-art-material

40. E. H. Kennard, Kinetic theory of gases, New York: McGraw-Hill, 1938

41. A. Agrawal and S. V. Prabhu, Survey on measurement of tangential momentum accommodation coefficient, *J. Vac. Sci. Technol. A* 26(4), 634 (2008)

42. N. Selden, N. Gimelshein, S. Gimelshein, and A. Ketsdever, Analysis of accommodation coefficients of noble gases on aluminum surface with an experimental/computational method, *Phys. Fluids* 21(7), 073101 (2009)

43. D. Ganta, E. B. Dale, J. P. Rezac, and A. T. Rosenberger, Optical method for measuring thermal accommodation coefficients using a whispering-gallery microresonator, *J. Chem. Phys.* 135(8), 084313 (2011)

44. S. Taguchi and K. Aoki, Rarefied gas flow around a sharp edge induced by a temperature field, *J. Fluid Mech.* 694, 191 (2012)

45. E. A. Guggenheim, Elements of the Kinetic Theory of Gases, Pergamon, New York, 1960